Metamorphic transformation rate over large spatial and temporal scales constrained by geophysical data and coupled modelling

György Hetényi, Kristel Chanard, Lukas P Baumgartner, Frédéric Herman

Received: 10 July 2020 | Revised: 10 March 2021 | Accepted: 11 March 2021

DOI: 10.1111/jmg.12604

ORIGINAL ARTICLE

Journal of METAMORPHIC GEOLOGY WILEY

Metamorphic transformation rate over large spatial and temporal scales constrained by geophysical data and coupled modelling

György Hetényi[1] | Kristel Chanard[1] | Lukas P. Baumgartner[1] | Frédéric Herman[2]

[1]Institute of Earth Sciences, Faculty of Geosciences and Environment, University of Lausanne, Lausanne, Switzerland

[2]Institute of Earth Surface Dynamics, Faculty of Geosciences and Environment, University of Lausanne, Lausanne, Switzerland

Correspondence
György Hetényi, Institute of Earth Sciences, Faculty of Geosciences and Environment, University of Lausanne, Lausanne, Switzerland.
Email: gyorgy.hetenyi@unil.ch

Funding information
Schweizerischer Nationalfonds zur Förderung der Wissenschaftlichen Forschung, Grant/Award Number: PP00P2_157627

Handling Editor: Bernardo Cesare

Abstract

Metamorphic transformation rates are classically determined on decimetre-scale field samples and from laboratory experiments at smaller scales. Here we present a geophysical approach based on field data and joint geophysical–petrological modelling to quantify the average rate of metamorphic transformations at the 10–100-kilometre and million-year scales. The model simulates the eclogitization of Indian lower crust as it penetrates beneath southern Tibet. Metamorphic transformation of the lower crust is tracked by its densification, the effect of which is then compared to observed gravity anomalies. From the modelling we find that the Indian lower crust's overall densification requires a partially hydrated initial composition. Moreover, the modelled evolution of this densification compared to what is predicted by pressure–temperature–density grids is consistent with delayed, far-from-equilibrium metamorphism. The Indian lower crust descends underneath the Himalaya until beneath southern Tibet in a thermodynamically metastable state until the first dehydration reactions are reached. This observation is used to determine the average rate of metastable rock transformation to an eclogite facies assemblage, constrained at between ~6×10^{-9} and 5×10^{-7} g/cm^2/year, and reaction affinity at 0.8–1.6 kJ/mol oxygen. Compared to field and laboratory data, this range of results matches the effective rates typically associated with regional metamorphism. This fit and correlation across the scales legitimates the use of transformation rates determined at small scales in large-scale geodynamic studies.

KEYWORDS

eclogitization, gravity anomaly, metamorphism, numerical modelling, transformation rates

Highlights

- Geophysical–petrological modelling of India's lower crust eclogite facies metamorphism.
- Average rock transformation rate estimates over long time- and large spatial scales.
- Results match reaction rates representative of regional metamorphism.
- Upscaling reaction rates for geodynamic models is feasible.

1 | INTRODUCTION

Metamorphic reactions occur over a large range of pressure and temperature conditions and affect the structure and physical properties of the Earth in various contexts, including linking processes such as deformation across various scales (e.g. Ague et al., 1998; Taetz et al., 2018). The overall rate at which the rock transformations proceed is the product of two factors: the intrinsic mineralogical reaction kinetics, and the rate of external changes (such as pressure, temperature, and deformation; see e.g. Fisher, 1978). From the analysis of natural processes, Baxter et al. (2003) distinguishes two main metamorphic environments: contact metamorphism, in which the abundant free fluids are produced by reactions during relatively large temperature overstepping, which leads to faster overall transformation rates; and regional metamorphism, in which slow fluid release or fluid-poor conditions result in significantly slower effective rates (e.g. Baxter et al., 2003). Beyond fluids, the difference in heating rate contributes to the difference in overall kinetics of these two metamorphic environments. Laboratory measurement of net reaction kinetics match well the faster rates. This is due mainly to the use of powders, which have high free reaction surfaces when compared to realistic scenarios of coarser grains in a rock, and because of water saturated environments, which enhance diffusive transport. Compared to these, regional metamorphism proceeds at effective rates that are commonly reported to be seven orders of magnitude slower; they scale with temperature (Figure 1; Baxter et al., 2003).

One common feature of all existing metamorphic net transformation rate estimates is that they are derived from spatially small-scale (sub-centimetre to centimetre scale) observations. A major challenge is the extrapolation of inherently small-scale processes and the upscaling to large-scale models of geological or geodynamic evolution. Natural constraints on the rates characteristic of regional metamorphism are based on scales ranging from that of grains (Eppel & Abart, 1997) and porphyroblasts (e.g. Carlson et al., 1995; Eiler et al., 1995) to that of lithological contacts (Baxter & DePaolo, 2000) and sills (Skelton et al., 1997) in outcrops. These observations cover about six orders of magnitude (from 10^{-5} to 10^{1} m) in spatial scale, but extrapolations are often made to the 10^{4}–10^{5} m scales (e.g. Toussaint et al., 2004; Yamato et al., 2007).

Here we use a coupled geophysical–petrological model to deduce apparent metamorphic rates at the 10–100 km scale. Inherently, this means we focus on large spatial- and long (*c*. million year) time-averaged transformation rates, and do not model grain-scale processes and their localization.

The context we consider is the lower crust of the India plate as it underthrusts the Tibetan Plateau from the south, as imaged by seismic methods (e.g. Nabelek et al., 2009; Subedi et al., 2018). Along its underthrusting path, the lower crust undergoes eclogite facies metamorphism (Henry et al., 1997; Hetényi et al., 2007). The dehydration reactions involved in eclogite facies metamorphism (Hetényi et al., 2007) coincide with the location of earthquakes at 50–80 km depth (Figure 2; Monsalve et al., 2006). Detailed focal mechanism analysis of a magnitude 4 event reveals an opening crack component, interpreted as dehydration embrittlement, which suggests there may be a causal link between eclogitization and seismicity (Alvizuri & Hetényi, 2019). The progress of overall metamorphic transformation of the lower crust can be tracked by its related increase in density, which produces a primary signal in gravimetry—comparable to that of the crust–mantle boundary. This can therefore be mapped by gravity anomalies observed at the surface (Figure 2). Here we use a coupled thermo-kinematic–metamorphic model to track this densification and compare it to the observed gravity anomalies. The presented model is an improvement and refinement of our earlier model (Hetényi et al., 2007), and

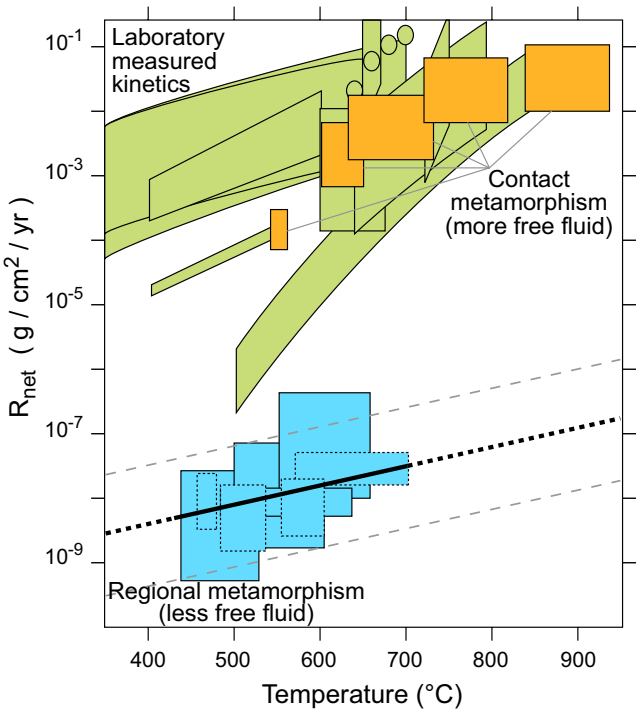

FIGURE 1 Overview of net metamorphic transformation rates R_{net} for high temperature (>400°C) systems, redrawn from Baxter et al. (2003). The three different types of data sets derived from small spatial scales (10^{-5} to 10^{1} m) are shown in colour. Green: laboratory measured kinetics based on 10 different publications. Orange: natural constraints on contact metamorphism based on two publications. Blue: natural constraints in regional metamorphism: dashed boxes are derived from direct garnet growth rate measurements (four publications), solid line boxes are from modelling of garnet growth (three publications) and solid–fluid Sr isotope exchange rate (one publication). The best-fit line (with uncertainties of the fit) is shown for regional metamorphism net rate estimates. See Baxter et al. (2003) for the full description and references [Colour figure can be viewed at wileyonlinelibrary.com]

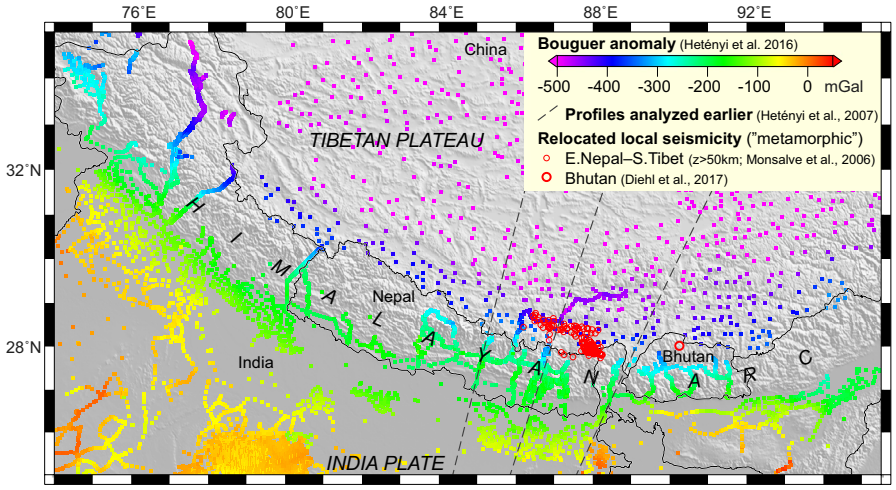

FIGURE 2 Study area showing the most recent compilation of Bouguer anomaly data (Hetényi et al., 2016) and seismicity that is proposed to be related to metamorphic reactions of the underthrusting India plate lower crust. The map shows very-high-quality event locations deeper than 50 km depth, relocated from temporary local networks (Diehl et al., 2017; Monsalve et al., 2006). Other such events may exist along the Himalaya but are not reported with high-quality locations. Among the three profiles analysed earlier (Hetényi et al., 2007) the best-constrained westernmost one is further scrutinized in this study (Figure 3) [Colour figure can be viewed at wileyonlinelibrary.com]

combines well-constrained thermo-kinematic parameters with petrogenetic grids to produce density models (Figure 3). Among the improvements, the numerical implementation of the thermal field is more realistic (Section 2.1.1), and we refine the spatial resolution to evaluate the location and length of the overall lower crustal densification of various models using field gravity data. We also consider model uncertainties with respect to those of the gravity data, which thereby constrain the order-of-magnitude rate of metamorphic reactions apparent at large spatial scales and averaged over long temporal scales.

2 | MATERIALS AND METHODS

2.1 | Modelling approach

We further develop the model based on that of Hetényi et al. (2007). The model structure is based on seismologically imaged lithosphere geometries such as the Moho and the upper crust–lower crust boundary (Nabelek et al., 2009). The kinematic and thermal field, as well as the implementation of the Main Himalayan Thrust is adapted from Bollinger et al. (2006). The model unit densities result from coupling thermo-kinematic and petrogenetic models. From this, synthetic gravity profiles are calculated, which are constrained by the most recent, comprehensive field gravity data set (Hetényi et al., 2016). Hetényi et al. (2007) demonstrated the validity of such models for three profiles across the Himalaya (Figure 2). In this study, we focus on the geophysically and geologically best-constrained profile across Central Nepal (Figures 2 and 3).

2.1.1 | Thermo-kinematic model

We newly implemented a 2D thermo-kinematic modelling tool to calculate the temperature–pressure field by solving the transient heat equation, including contributions from internal heat generation, as well as with advective and conductive heat transport (Carslaw & Jaeger, 1959):

$$\rho C_p \left(\frac{\partial T}{\partial t} + \vec{v} \cdot \nabla T \right) = \nabla \cdot (k \nabla T) + H_R + H_S$$

where ρ is the material density, C_p and k the isobaric heat capacity and thermal conductivity respectively, $\vec{v}$ the local velocity, T the temperature, and t time. H_R and H_S correspond to the radiogenic heat production and the shear heating. The equation is solved in finite differences using an explicit scheme (Crank, 1975; Gerya, 2010) on a regular rectangular grid. The code is explicit and we use a time step that is sufficiently small to ensure stability and to limit numerical diffusion. The shear heating source term is computed as described by Bollinger et al. (2006) and Herman et al. (2010).

The model's thermal and velocity set-up (Figure 3a) are based on Bollinger et al. (2006). The velocity field is constructed in order to satisfy the continuity equation, it accounts for 21 mm/year (e.g. Lavé & Avouac, 2000) convergence and an accretion window to allow growth of the orogenic wedge (Figure 3). The model of Bollinger et al. (2006) was chosen as it reproduces the inverse metamorphic gradient, peak temperatures, and exhumation ages deduced from large field data sets across the Central Nepal Himalaya. The implementation of the thermal field is improved with respect to earlier models: the basal heat flow boundary condition is set at varying depth

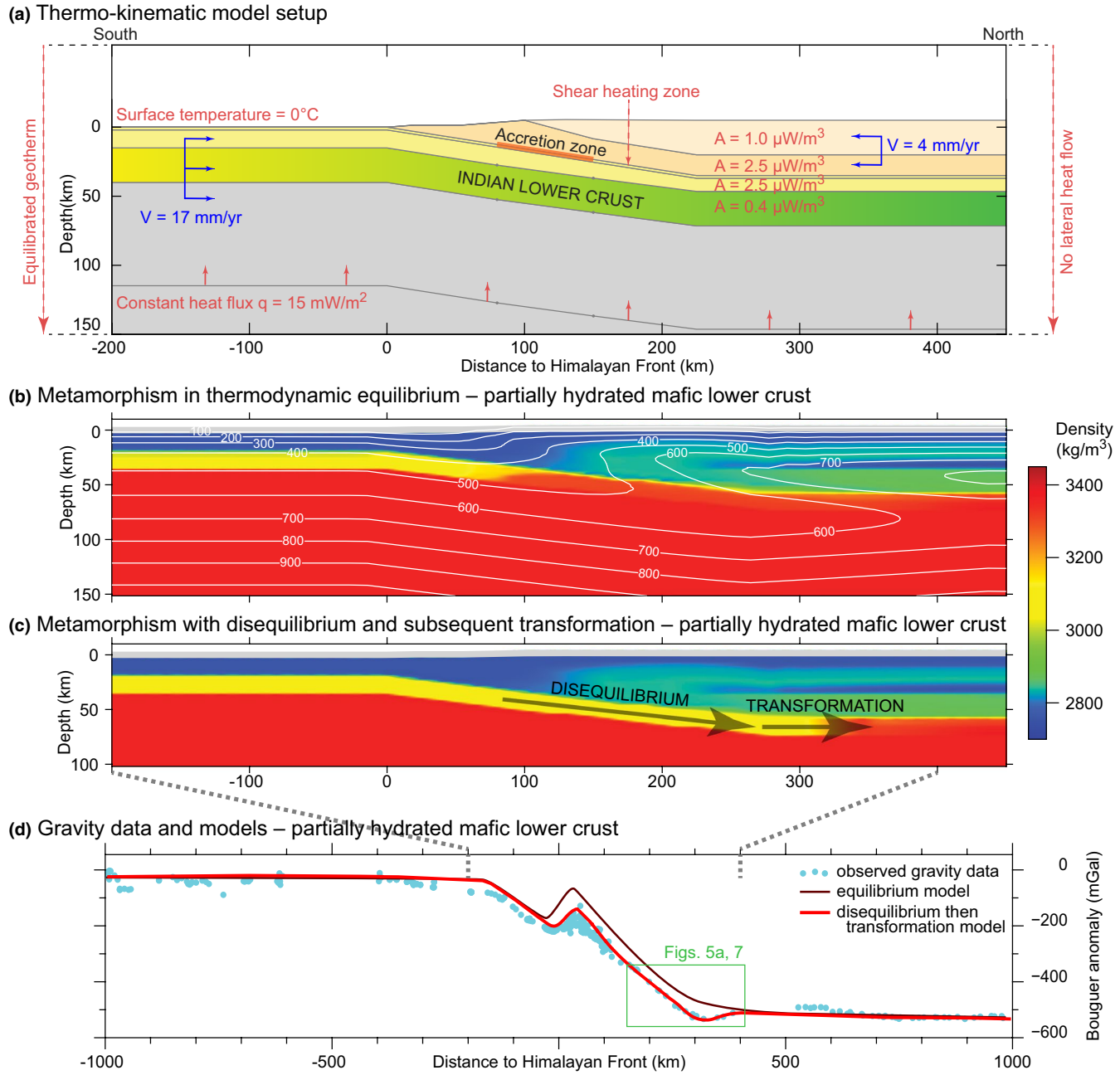

FIGURE 3 (a) Thermo-kinematic model set-up. Thermal boundary conditions are shown in red. Imposed convergence rate is shown in blue, additional features are described in the text. (b) Thermal and density fields assuming metamorphic reactions at equilibrium for the partially hydrated (1 wt%) model. (c) Modified density model when accounting for thermodynamic disequilibrium of the Indian lower crust and subsequent transformation, for which we estimate the large spatial- and long-time-averaged rate. (d) Bouguer gravity anomaly data and profiles of synthetic values from the models shown in (b) and (c) [Colour figure can be viewed at wileyonlinelibrary.com]

along the profile. In addition, thermal conductivity of units varies as a function of temperature following (Whittington et al., 2009). Heat capacity C_p is pressure and temperature dependent in the Indian lower crust, as a property computed in the petrogenetic grid (see Section 2.1.2). Radiogenic heat production is the best-fit values from results of Hetényi et al. (2007). Uncertainties are discussed in Section 3.3 and in Hetényi et al. (2007).

The topography is assumed to be in steady state, meaning that erosion compensates exactly the rock uplift rate everywhere. There is no horizontal conductive heat flow across vertical (e.g. the left and right) model boundaries. The imposed horizontal velocities are uniform within the footwall and hangingwall respectively. The model evolves over 50 Ma when the temperature and pressure field are taken for further calculations, which is representative for Tibet's current state.

The modelled domain extends from −400 to 650 km distance, only the zone of interest is shown in Figure 3a–c. The gravity profile is shown from −1,000 to 1,000 km distance to show the far-field fit which is the primary criteria to match in modelling. The model's mesh resolution is 5 km in horizontal and 1 km in vertical direction.

2.1.2 | Petrological model

The modelling of the Indian lower crust includes pressure–temperature–composition-dependent physical properties, most importantly density for the gravity model, but also heat capacity. The properties of equilibrium assemblages were calculated using the Perple_X software (Connolly, 2005; Connolly & Podladchikov, 2009). It is based on minimizing Gibbs free energy.

There is a lack of direct rock samples of Indian lower crust in our study area. Outcrops from the exposed Indian shield several hundreds or thousands of kilometres towards the south likely represent very different terrains than those currently beneath the Himalaya. Therefore, it is reasonable to assume an average continental lower crust composition (Rudnick & Gao, 2003; Rudnick & Fountain, 1995). In addition, as in our earlier model, we consider three levels of hydration: dry, fully saturated, and partially hydrated (taken at 1 wt%). A dry lower crust would react with water from external sources, as considered for the context of the Caledonides (e.g. Austrheim, 1987), although the granulites there are typically not totally dry (Rockow et al., 1997; H. Austrheim personal communications 2019 and 2020).

For the modelling, the respective compositions (Rudnick & Gao, 2003; Rudnick & Fountain, 1995) and selected solid solution models are given in Tables 1 and 2. The calculated density grids for the three models as a function of temperature and pressure are shown in Figure 4. For the partially hydrated and water saturated models, we assume that free fluids produced during dehydration reactions are extracted from the system along preferential pathways (possibly along structural/lithologial heterogeneities at the meso-scale) more rapidly than they could react with other rocks; hence the density grids represent the values of the solid phase. Therefore, the partially hydrated calculations are water undersaturated rocks until first dehydration reactions occur within them to produce free water. The stable phase assemblage at water saturation is composed of clinopyroxene+phengite+amphibole+garnet+zoisite+quartz+water. Amphibole is present in all stability fields along the pressure–temperature path of the Indian lower crust, and carries, along with zoisite and/or biotite, the water in this model.

The densities of the other units used in our thermokinematic modelling (the upper crust and the mantle) are based on the petrogenetic grids of Bousquet et al. (1997), and the model considers equilibrium conditions for these units.

TABLE 1 Petrological composition considered for the Indian Lower Crust (wt%), after Rudnick and Fountain (1995) and Rudnick and Gao (2003), for three levels of hydration: dry, fully saturated, and partial hydration (1 wt%). The amount of water in the fully saturated model depends on pressure and temperature; for the Indian lower crust's *P–T* path in the model, it increases from **~0**.25 to **~5** wt%, and it is **~3** wt% where it starts underthrusting. The H_2O present in the system proportionally decreases the values of the various oxides in the fully saturated case

Component	Dry	Fully saturated	Partially hydrated
SiO_2	53.961	53.961	53.422
Al_2O_3	17.078	17.078	16.907
FeO	8.660	8.660	8.573
MgO	7.316	7.316	7.243
CaO	9.691	9.691	9.594
Na_2O	2.678	2.678	2.651
K_2O	0.616	0.616	0.610
H_2O	0.000	saturated	1.000

2.1.3 | Gravity model

The density field resulting from the coupled thermokinematic–petrological model is used to compute 2D gravity anomalies along the profile, which are then compared to field data. To calculate synthetic Bouguer anomalies, we implement the algorithm of Won and Bevis (1987), based on the method of Talwani et al. (1959) which considers polygons' vertices and sums up their respective gravitational effects at a given observation site.

The gravity data in this study are from the regional land gravity data compilation of Hetényi et al. (2016) (Figure 2), which includes new data (Berthet et al., 2013; Hammer et al., 2013) acquired since the publication of our earlier data set. The data set shows general across-orogen crustal thickening towards the Tibetan Plateau, and reveals lateral structural variations that are mainly inherited from the India plate.

2.2 | Metamorphic rate estimate

2.2.1 | Average transformation rate

To impose bounds on the range of rates apparent at large spatial- and long time-scales, we estimate the overall transformation rate of the Indian lower crust by analysing the horizontal distance over which densification occurs. This is tested by varying the distance within which lower crustal density in the model progresses from its initial low to its final high value, while the computed gravity anomaly is required to fit the observed data within its uncertainty. The shorter this transformation distance, L_{TR}, the

Solution	Formula	Reference
Biotite	$K[Mg_xFe_yMn_{1-x-y}]_{3-w}Al_{1+2w}Si_{3-w}O_{10}(OH)_2$, $x + y \leq 1$	Powell and Holland (1999)
Orthopyroxene	$[Mg_xFe_{1-x}]_{2-y}Al_{2y}Si_{2-y}O_6$	Holland and Powell (1996)
Clinopyroxene	$Na_{1-y}Ca_yMg_{xy}Fe_{(1-x)y}Al_ySi_2O_6$	Holland and Powell (1996)
Clinoamphibole	$Ca_{2-2w}Na_{z+2w}[Mg_xFe_{1-x}]_{3+2y+z}Al_{3-3y-w}Si_{7+w+y}O_{22}(OH)_2$, $w + y+z \leq 1$	Wei and Powell (2003), White et al. (2003)
Garnet	$Fe_{3x}Ca_{3y}Mg_{3z}Mn_{3(1-x-y-z)}Al_2Si_3O_{12}$, $x + y+z \leq 1$	Holland and Powell (1998)
Feldspar	$K_yNa_xCa_{1-x-y}Al_{2-x-y}Si_{2+x+y}O_8$, $x + y \leq 1$	Fuhrman and Lindsley (1988)
Talc	$[Mg_xFe_{1-x}]_{3-y}Al_{2y}Si_{4-y}O_{10}(OH)_2$	
Sapphirine	$[Mg_xFe_{1-x}]_{4-y/2}Al_{9-y}Si_{2-y/2}O_{20}$	Holland and Powell (1998)
Chloritoid	$Mg_xFe_yMn_{1-x-y}Al_2SiO_5(OH)_2$, $x + y \leq 1$	White et al. (2000)
Chlorite	$[Mg_xFe_wMn_{1-x-w}]_{5-y+z}Al_{2(1+y-z)}Si_{3-y+z}O_{10}(OH)_8$, $x + w \leq 1$	Holland et al. (1998)
White mica	$K_yCa_xNa_{1-x-y}(Mg_{1-v}Fe_v)_zMg_wTi_wAl_{3+x-w-z}Si_{3-x+z}O_{10}(OH)_2$, $x + y \leq 1$, $w + z \leq y$	Auzanneau et al. (2010), Coggon and Holland (2002)

TABLE 2 Selected solid solution models for petrological modelling. The thermodynamic data used by the Perple_X code are based on Holland and Powell (1998, updated in 2002). The compositional variables w, x, y, and z may vary between zero and unity and are determined in Perple_X as a function of computational variables by Gibbs free energy minimization

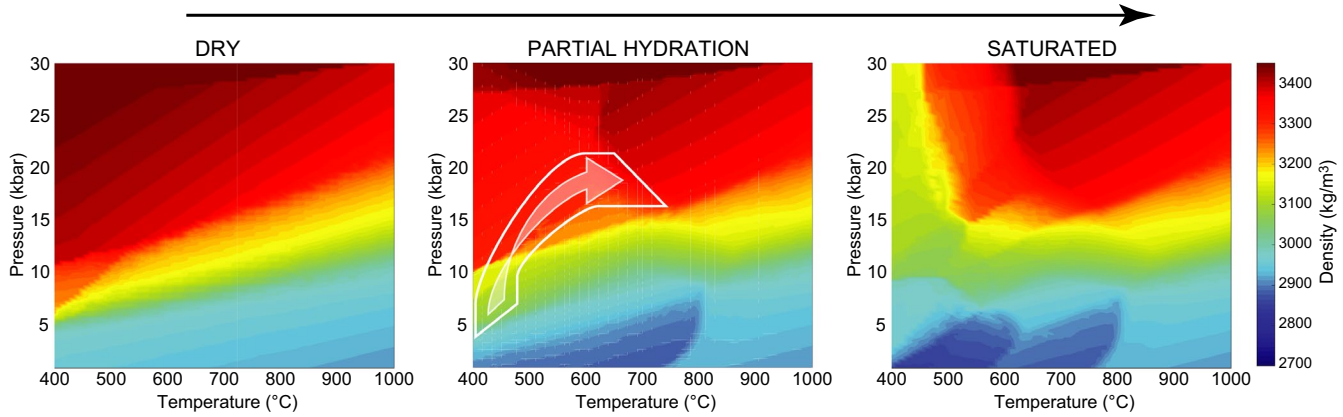

FIGURE 4 Density grids of the solid phase as a function of temperature and pressure for the three selected hydration levels of the Indian lower crust, calculated with the Perple_X software suite (see text for details). The *P–T* path of the Indian lower crust as it underthrusts southern Tibet is shown with a white contour including an arrow, going through blueschist facies conditions to reach eclogite facies conditions
[Colour figure can be viewed at wileyonlinelibrary.com]

faster the average rate, and vice versa (Figure 5a). The onset and completion points defining L_{TR} are located symmetrically to the central location of this transformation zone, C_{TR}, which is varied independently since we consider non-transformation of the Indian lower crust (see below). To quantify the large-scale, time-averaged transformation rate and to compare it to field- and laboratory-based results (Figure 1), we make our interpretations in the following frame:

- In a unit time t, a total rock volume V undergoes reactions;
- The rock is assumed to be composed of spherical grains of radius r;
- The number of grains in the volume is $n = V/(4/3{\cdot}\pi{\cdot}r^3)$;
- The total surface of these spheres on which reactions take place is then $n{\cdot}4{\cdot}\pi r^2 = 3{\cdot}V/r$; as an approximation, grain size is not varied during reaction progress;
- The mass of produced eclogite facies rock of density ρ in the same volume is $\rho{\cdot}V$;
- The transformation rate is mass/surface/time: $R_{TR} = \rho{\cdot}r/(3{\cdot}t)$;
- In the context of Indian lower crust, time is obtained from the transition length L_{TR} in the model, divided by the underthrusting rate v, so ultimately $R_{TR} = \rho{\cdot}r{\cdot}v/(3{\cdot}L_{TR})$.

In summary, in this model the large-scale, long-time-averaged reaction rate depends on four factors, two of

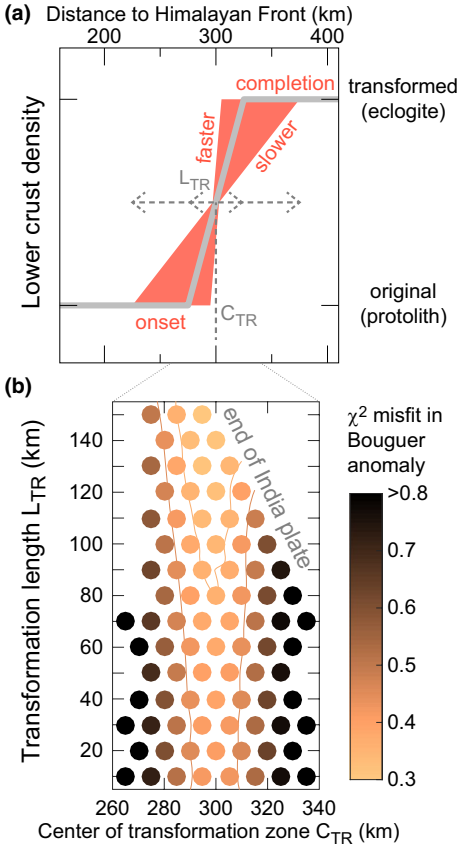

FIGURE 5 (a) Scheme of testing various reaction rates by independently changing the central position C_{TR} and length L_{TR} of the transformation zone, defined between the onset and completion of lower crustal densification. The grey dashed lines and arrows illustrate that the transformation zone is centred at C_{TR} and its length varies symmetrically to it. (b) Misfit between synthetic and observed gravity data around the eclogitization zone as a function of the centre and length of the transformation zone (see also Figure 7). Misfit iso-contours at 20% and at 50% higher than that of the best model (χ^2 ~0.3) are shown for reference [Colour figure can be viewed at wileyonlinelibrary.com]

which we keep constant (ρ = 3,300 kg/m^3, v = 17 mm/year), one is varied systematically (r = 0.5–5 mm based on our field experience worldwide and on examples in the literature, e.g. Ahrens & Schubert, 1975; Corti et al., 2019), and L_{TR} is taken from the simulations that fit the gravity data within uncertainty. This order-of-magnitude estimate for regional-scale average transformation rate is then compared to existing estimates from hand-sample- and outcrop-scale studies.

We note that the long-term densification of the Indian lower crust means that, by conservation of mass, the volume of corresponding rocks decreases. This has significant effects on the stress field and the deformation of an orogenic root (Heténi et al., 2011), but does not affect the validity of our thermo-kinematic model.

2.2.2 | Reaction affinity estimate

To better link our results to kinetic laws published in the petrological literature we estimate the chemical affinity of the eclogitization reaction based on the model's physical and petrological parameters. Affinity is the driving force for mineral reactions: it is zero at phase equilibrium, and transformation rate scales with its magnitude. The affinity is the difference in Gibbs free energy, G, between the equilibrium state and the actual state present in the rock (e.g. Roselle et al., 1997).

For the Indian lower crust, the free energy difference, ΔG, was calculated assuming the equilibrated mineralogy at the start of underthrusting. We calculated the free energy along the P–T path of this assemblage assuming constant volume, which is a reasonable approximation for an overstepped reaction, and an entropy changing with a constant heat capacity. Thus the equation to calculate the free energy difference, ΔG is approximated as $\Delta G = -\Delta T{\cdot}S + \Delta P{\cdot}V$, for which we retrieve values from the thermo-kinematic model and the petrogenetic grid. The affinity of reaction is then obtained as the difference between this calculated free energy, and the free energy of the stable assemblage at the initial pressure and temperature. We perform this affinity estimate along the path of the top, the middle and the bottom of the Indian lower crust, and take the range of values for the discussion, in the commonly used units of J/mol of oxygen.

3 | RESULTS AND DISCUSSION

The newly implemented model reproduces the two main findings of earlier results (Heténi et al., 2007). First, it constrains the initial level of Indian lower crust hydration, by comparing the three different hydration level models' gravity signal with the observations (see details in Section 3.1). Second, it emphasizes the role of disequilibrium: the density of the Indian lower crust remains relatively low beyond P–T conditions at which thermodynamic equilibrium would prescribe a density increase. The subsequent rate of densification fitting observations is investigated in Section 3.2.

3.1 | Composition of the lower crust

The level of initial hydration in the Indian lower crust is constrained by the far-field gravity anomaly difference between the southern and northern end of the model. The range of possible hydration state depends on the chosen rock chemistry, which is the average continental lower crustal composition of Rudnick and Fountain (1995) and Rudnick and Gao (2003). The far-field gravity anomaly difference is the first step to satisfy in density modelling before further details can be simulated. Of the three petrological models with different

hydration levels, the respective synthetic gravity profiles of the dry and saturated models do not reproduce the observed gravity anomaly difference between the far-field ends of the profile (Figure 6). The dry model produces too small a density change and the saturated model produces too large a density change during metamorphic transformation of the lower crust from onset to completion, and the >100 and respectively ~70 mGal difference of these two models from the data in S. Tibet (Figure 6) is significantly higher than data uncertainty. Therefore, based on these geophysical and modelling arguments, these two hydration-level models are discarded from further analysis. Only the partially hydrated model with 1 wt% water is able to reproduce the observed far-field gravity anomaly difference. This result is constrained by the density difference between the protolith and the transformed rock, as depicted by the starting and ending points of the Indian lower crust's *P*–*T* trajectory (Figure 4). Geologically, this is a reasonable estimate for a former granulite facies rock with partial hydration.

This result, highlighting the need for some degree of initial hydration of the Indian lower crust implies that this unit cannot be perfectly dry granulite, as proposed by for example Priestley et al. (2008) and Shi et al. (2018), but it has to be a partially hydrated rock to fit the gravimetric constraints related to densification caused by eclogitization. Furthermore, the rocks are brought to eclogite facies conditions through blueschist facies conditions, and not from granulite facies (see *P*–*T* path in Figure 4). On their path, these partially hydrated rocks cross dehydration reactions lines as they enter eclogite facies conditions, and amphibole+(clino)zoisite start to break down, releasing water. This, in turn, triggers the observed earthquakes while forming an eclogite facies rock (Alvizuri & Hetényi, 2019; Hetényi et al., 2007). This logic also takes away the need to invoke externally infiltrating fluids as drivers of eclogitization, unlike for the Bergen Arcs in the Norwegian Caledonides (Austrheim, 1987). The assumption of external fluids has been here replaced by an initial hydration condition of the Indian lower crust, which in turn could be tested and constrained by our model. The sustainability of deep crustal densification is different from what is proposed in case of direct fluid import (e.g. Malvoisin et al., 2020): it is here provided by the continued input of Indian lower crustal material.

The partially hydrated model still features a large zone of misfit between observed and synthetic gravity data at ~−50 to 400 km distances (Figures 3b,d and 6). This discrepancy is resolved when non-equilibrium metamorphism is taken into account: the Indian lower crust, in the absence of free water in the system, remains in an out-of-equilibrium state, and keeps its density lower than it would be in equilibrium conditions; this adjusts the bulk of the synthetic anomalies to fit the gravity data, as in Hetényi et al. (2007). However, the subsequent large-scale and long-time averaged reaction rate remains to be constrained in order to fit the local minimum in gravity anomalies at ~300 km distance (Figure 3c,d).

3.2 | Gravimetric constraints on metamorphic transformation rate

The rate at which metamorphic transformations proceed once the Indian lower crust in thermodynamic disequilibrium starts to metamorphically transform and densify is investigated by a parametric search as explained in Section 2.2.1 and Figure 5. This is a new search as in our earlier model (Hetényi et al., 2007) the transformation rate was assumed to be the same as if it occurred progressively following thermodynamic equilibrium conditions.

We therefore perform a spatially high-resolution (10 km) grid test on the positions of the onset and completion of lower crustal densification, which allow to deduce the transformation rate (Figure 5). The misfit between observed data *Gobs* and synthetic data *Gcal* in terms of gravity anomalies is quantitatively assessed as.

$$\chi^2 = \frac{\sum_i^N \left(\frac{\mathrm{Gobs}_i - \mathrm{Gcal}_i}{G\sigma_i} \right)^2}{N}.$$

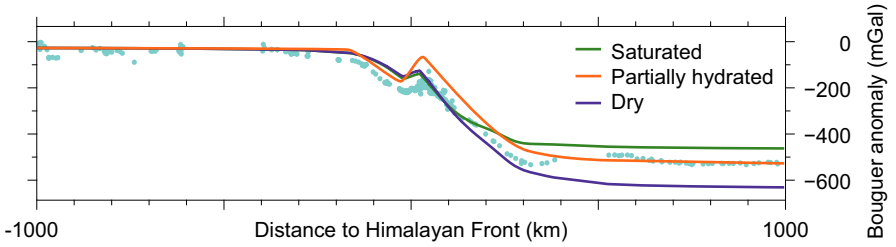

FIGURE 6 Gravimetric control on the initial hydration level of the modelled Indian lower crust. Bouguer anomalies must first fit the far-field difference between the left and right ends of the profile before adjusting inner parts of the model. The large misfit between observed data (blue dots) as well as the dry and saturated composition models precludes the further use of these two models. The partially hydrated lower crustal composition model fits the far-field difference in gravity anomaly, and is further refined to fit the observed data in the central portion of the profile [Colour figure can be viewed at wileyonlinelibrary.com]

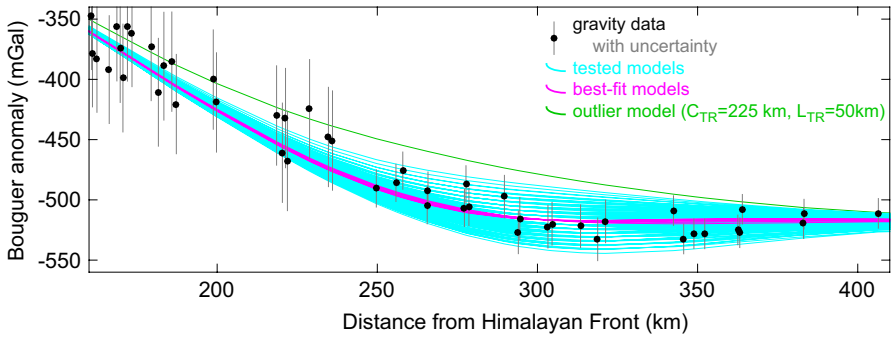

FIGURE 7 Synthetic gravity anomaly profiles computed from the coupled modelling results and their fits to the observed data and their uncertainty. All tested models' misfit is represented on Figure 5b, except that of the outlier model. The window shown (from 160 to 410 km distance) is where the misfits were calculated as the gravity anomalies were found to be most sensitive to the metamorphic reaction (i.e. densification) in that range. Longer windows produced the same pattern of results [Colour figure can be viewed at wileyonlinelibrary.com]

where $G\sigma$ is the uncertainty of the observed data, and N the number of data points. Figure 7 shows the data points and fits of tested models in the zone of interest for lower crustal densification.

The misfit map as a function of central location and length of the transformation zone (Figure 5b) demonstrates that several models produce similarly good fits. Their common feature is that the densification zone (between the onset and completion points) is centred at 300 km horizontal distance. The range of transformation distances L_{TR} is between 20 and 150 km. Longer transformation distances are possible, but fail to fit several gravity data points and the local minimum. Shorter transformation distances are possible but not reliably resolvable by our gravity data, and the L_{TR} = 20-km-model fits slightly less well than the L_{TR} = 150-km-model, hence we retain this range of possible solutions. Models with longer L_{TR} are excluded as the extent of the Indian lower crust is limited towards the north (Nabelek et al., 2009). Other models where the transition is not centred on 300 km distance perform worse in simulating the gravity data (see one example in Figure 7).

Replacing this range of L_{TR} values in the equation $R_{TR} = \rho \cdot r \cdot v / (3 \cdot L_{TR})$ introduced in Section 2.2.1, we obtain average transformation rates ranging between 6×10^{-9} and 5×10^{-7} g/cm^2/year. This spans ~2 orders of magnitude: one stems from the found range of L_{TR} values, and one from the assumed grain radii. Ultimately, this large-scale long-time-averaged transformation rate is compared to laboratory- and field-based studies. Our results, constrained by geophysical data and a joint petrological–geophysical modelling approach on the 10–100 km scale, match very well the rates characteristic of regional metamorphism determined at small spatial scales (Figure 8). Our finding has two major consequences discussed below.

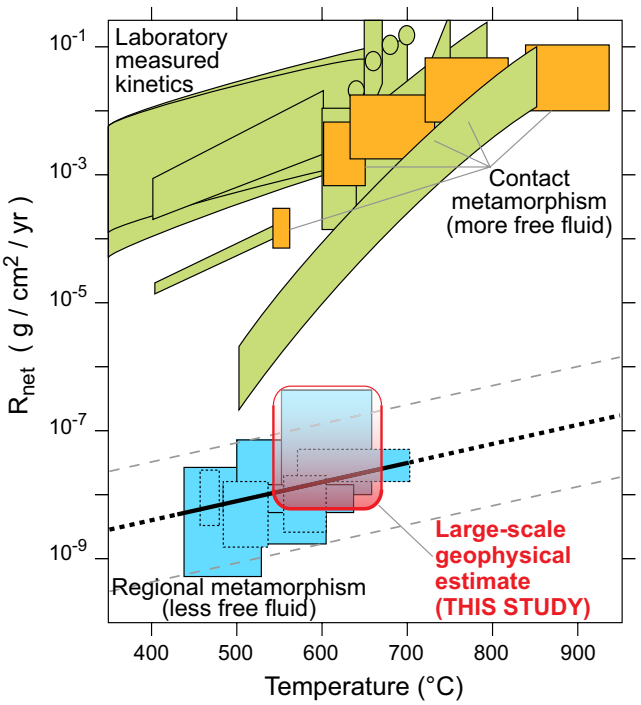

FIGURE 8 Overview of metamorphic transformation rates, as presented in Figure 1 following Baxter et al. (2003) and results of this study added in red. Our results deduced on spatially large scales (10^4–10^5 m) and averaged over long (~ 1 Ma) time-scales represent the eclogitization of the partially hydrated Indian lower crust along a prograde path, along with its densification and complete dehydration agrees exceptionally well with the regional metamorphic trend [Colour figure can be viewed at wileyonlinelibrary.com]

3.3 | Implication for regional metamorphism

For regional metamorphism in general: the match of transformation rates across several spatial scales validates the common practice of upscaling, in which reaction rates deduced at small scale are applied to larger scale geological and geodynamical models. Our large-scale results find good agreement with metamorphic reaction rates for small-scale environments in which fluids are not always available. In fact, the rates in this study, for prograde densification and dehydration of the lower crust, compare

well with observed regional metamorphic rates, mainly documented by garnet growth (Figure 8), where reactions are limited by fluid transport. The rate of overstepping characteristic for the present case is that reported in many regional metamorphic settings (e.g. John & Schenk, 2003; Wolfe & Spear, 2017). Hence the resulting microscopic textures—grain size, number of nuclei—in the present case are all likely similar to typical regional metamorphic rocks. Future numerical modelling work can incorporate such rates when implementing metamorphic phase changes together with their density and volume changes (Hetényi, 2014; Hetényi et al., 2011). Further development in modelling that connect processes across scales should include the actual mechanisms of transport-limited reaction rates considering porosity, pore connectivity, chemical composition, and solubility (e.g. Kelly et al., 2013) in order to obtain more accurate kinetic rates.

Our estimated values of affinity are between 0.8 and 1.6 kJ/mol oxygen (O) with lower values at shallower and higher values at deeper levels of the underthrusted Indian lower crust. These values fit very well within the range given of 0.3–0.6 kJ/mol O from the most recent estimates for regional metamorphic garnet growth by Wolfe and Spear (2017) for garnet nucleation during Barrovian metamorphism in the Connecticut Valley Synclinorium (USA), and 2.0–2.4 kJ/mol O found by Castro and Spear (2016) for the nucleation of garnet in the Cyclades subduction complex on Sifnos (Greece). This further strengthens the argument that geophysically and petrologically deduced reaction rates are scalable in space.

3.4 | Implication for the Indian lower crust

For the case of the Indian lower crust: the match means that the fluid-poor context of regional metamorphism can be realistically applied. This implies the transience of metamorphic dehydration events, after which the fluids are rapidly expelled from the rock through fractures, along lithological layering, porosity waves (e.g. Connolly & Podladchikov, 2015), reactive fluid flow (e.g. Zack & John, 2007), or reactive porosity waves (e.g. Malvoisin et al., 2015). These fluid-driven episodes could cluster in time and could relate to periods of regional, intermediate-depth seismicity (as e.g. the one observed in Monsalve et al. 2006) as a consequence of metamorphic transformations (Alvizuri & Hetényi, 2019), thus interrupting longer, quiescent periods when fluid availability is limited. Lateral heterogeneities in thermal structure or/and in composition of the Indian lower crust may exist (and if so, could be inherited) and could control the spatial extent of fluid presence within the Indian lower crust and, possibly, the lateral extent of deep-crustal metamorphic earthquake occurrence (Figure 2).

3.5 | Numerical model uncertainty assessment

The possible range of thermal fields still fitting the surface constraints varies by ~±50°C at lower crustal depths, and this corresponds to ~50 km uncertainty in the horizontal location of densification (Bollinger et al., 2006; Hetényi et al., 2007). We consider the pressure of the underthrusted lower crust to be properly estimated at ±1 kbar given the model's numerical discretization (this model does not account for possible effects due to variations in gravitational potential energy, see e.g. Schmalholz et al., 2019). The variation of the modelled *P–T* range can be compensated by slightly different amounts of water in the partially hydrated compositional model, which may affect the location of the dehydration reactions in *P–T* space. None of these model uncertainties will significantly affect the deduced transformation rates as the transformation lengths remain on the order of few to a dozen 10s of kilometres.

4 | CONCLUSIONS

The first estimate of large spatial- and long-time-averaged metamorphic transformation rates is presented in this study. The analysis is based on a physico-chemical model coupling various geophysical and geological data, and on the case study of Indian lower crust eclogitization. The modelling is carried out at high spatial resolution and takes into account uncertainties, especially regarding the distance over which lower crustal densification occurs. The inferred order-of-magnitude transformation rates match the rates characteristic of regional metamorphism known from classical metamorphic petrology. The results fit well with the limited fluid availability, for example, a partially hydrated lower crust and its subsequent dehydration at high temperatures. Moreover, the upscaling in the use of effective metamorphic rates, hitherto determined at small spatial scales, is justified. An estimate of reaction affinity and good match with values deduced classically at small spatial scales points to the same conclusion.

The available regional gravity data set (Figure 2) enables the assessment of along-strike variations of our findings. This may shed light on the 3D variability of metamorphic transformation rates as well as of the composition of the lower crust beneath the Himalaya in future work.

ACKNOWLEDGEMENTS

We greatly acknowledge discussions with and input from Håkon Austrheim, Ethan Baxter, Barbara Dutrow, Tom Foster, Djordje Grujic, Benjamin Malvoisin, and Timm John. The help of Aleksandar Licul and Yury Podladchikov in the thermo-kinematic model development is appreciated. Thanks to Jamie Connolly for Perple_X (available at http://www.

perplex.ethz.ch). Constructive comments and suggestions from three reviewers clearly improved the manuscript; we thank all of them as well as the Editor for their time and work. We are grateful to the Swiss National Science Foundation for funding project OROG3NY through grant PP00P2_157627. The authors declare to have no competing financial interests. All data used in this study are available in the cited literature.

ORCID

György Hetényi https://orcid.org/0000-0001-9036-4761

REFERENCES

Ague, J. J., Park, J., & Rye, D. M. (1998). Regional metamorphic dehydration and seismic hazard. *Geophysical Research Letters*, *25*, 4221–4224. https://doi.org/10.1029/1998GL900124

Ahrens, T. J., & Schubert, G. (1975). Gabbro-eclogite reaction rate and its significance. *Reviews of Geophysics and Space Physics*, *13*, 383–400.

Alvizuri, C., & Hetényi, G. (2019). Source mechanism of a lower crust earthquake beneath the Himalayas and its possible relation to metamorphism. *Tectonophysics*, *769*, 128153. https://doi.org/10.1016/j.tecto.2019.06.023

Austrheim, H. (1987). Eclogitization of lower crustal granulites by fluid migration through shear zones. *Earth and Planetary Science Letters*, *81*, 221–232. https://doi.org/10.1016/0012-821X(87)90158-0

Auzanneau, E., Schmidt, M. W., Vielzeuf, D., & Connolly, J. A. D. (2010). Titanium in phengite: A geobarometer for high temperature eclogites. *Contributions to Mineralogy and Petrology*, *159*, 1–24. https://doi.org/10.1007/s00410-009-0412-7

Baxter, E. F. (2003). Natural constraints on metamorphic reactions rates. In: D. Vance, W. Müller, & I. Villa (Eds.) *Geochronology: Linking the isotopic record with petrology and textures*. *Geological Society of London Special Publications*, *220*, 183–202.

Baxter, E. F., & DePaolo, D. J. (2000). Field measurement of slow metamorphic reaction rates at temperatures of 500° to 600°C. *Science*, *288*, 1411–1414. https://doi.org/10.1126/science.288.5470.1411

Berthet, T., Hetényi, G., Cattin, R., Sapkota, S. N., Champollion, C., Kandel, T., Doerflinger, E., Drukpa, D., Lechmann, S., & Bonnin, M. (2013). Lateral uniformity of India plate strength over Central and Eastern Nepal. *Geophysical Journal International*, *195*, 1481–1493. https://doi.org/10.1093/gji/ggt357

Bollinger, L., Henry, P., & Avouac, J.-P. (2006). Mountain building in the Nepal Himalaya: Thermal and kinematic model. *Earth and Planetary Science Letters*, *244*, 58–71. https://doi.org/10.1016/j.epsl.2006.01.045

Bousquet, R., Goffé, B., Henry, P., Le Pichon, X., & Chopin, C. (1997). Kinematic, thermal and petrological model of the Central Alps: Lepontine metamorphism in the upper crust and eclogitisation of the lower crust. *Tectonophysics*, *273*, 105–127. https://doi.org/10.1016/S0040-1951(96)00290-9

Carlson, W. D., Denison, C., & Ketcham, R. A. (1995). Controls on the nucleation and growth of porphyroblasts: Kinetics from natural textures and numerical models. *Geological Journal*, *30*, 207–225. https://doi.org/10.1002/gj.3350300303

Carslaw, H. S., & Jaeger, J. C. (1959). *Conduction of heat in solids*. Oxford University Press, pp. 1–510.

Castro, A. E., & Spear, F. S. (2016). Reaction overstepping and reevaluation of peak P-T conditions of the blueschist unit Sifnos, Greece: Implications for the cyclades subduction zone. *International Geology Review*, *59*, 548–562. https://doi.org/10.1080/00206814.2016.1200499

Coggon, R., & Holland, T. J. B. (2002). Mixing properties of phengitic micas and revised garnet-phengite thermobarometers. *Journal of Metamorphic Geology*, *20*, 683–696. https://doi.org/10.1046/j.1525-1314.2002.00395.x

Connolly, J. A. D. (2005). Computation of phase equilibria by linear programming: A tool for geodynamic modeling and its application to subduction zone decarbonation. *Earth and Planetary Science Letters*, *236*, 524–541. https://doi.org/10.1016/j.epsl.2005.04.033

Connolly, J. A. D., & Podladchikov, Y. Y. (2009). The geodynamic equation of state: What and how. *Geochemistry Geophysics Geosystems*, *10*, Q10014. doi:10.1029/2009GC002540

Connolly, J. A. D., & Podladchikov, Y. Y. (2015). An analytical solution for solitary porosity waves: Dynamic permeability and fluidization of nonlinear viscous and viscoplastic rock. *Geofluids*, *15*, 269–292. https://doi.org/10.1111/gfl.12110

Corti, L., Zucali, M., Visalli, R., Mancini, L., & Sayab, M. (2019). Integrating X-ray computed tomography with chemical imaging to quantify mineral re-crystallization from granulite to eclogite metamorphism in the Western Italian Alps (Sesia-Lanzo Zone). *Frontiers in Earth Sciences*, *7*, 327. https://doi.org/10.3389/feart.2019.00327

Crank, J. (1975). *The mathematics of diffusion*, 2nd ed. 143.

Diehl, T., Singer, J., Hetényi, G., Grujic, D., Clinton, J., Giardini, D., & Kissling, E.; GANSSER Working Group. (2017). Seismotectonics of Bhutan: Evidence for segmentation of the Eastern Himalayas and link to foreland deformation. *Earth and Planetary Science Letters*, *471*, 54–64. https://doi.org/10.1016/j.epsl.2017.04.038

Eiler, J. M., Valley, J. W., Graham, C. M., & Baumgartner, L. P. (1995). Ion microprobe evidence for the mechanisms of stable isotope retrogression in high-grade metamorphic rocks. *Contributions to Mineralogy and Petrology*, *118*, 365–378. https://doi.org/10.1007/BF00461404

Eppel, H., & Abart, R. (1997). Grain-scale stable isotope disequilibrium during fluid-rock interaction. 2: An example from the Penninic-Austroalpine tectonic contact in eastern Switzerland. *American Journal of Science*, *297*, 707–728. https://doi.org/10.2475/ajs.297.7.707

Fisher, G. W. (1978). Rate laws in metamorphism. *Geochimica et Cosmochimica Acta*, *42*, 1035–1050. https://doi.org/10.1016/0016-7037(78)90292-2

Fuhrman, M. L., & Lindsley, D. H. (1988). Ternary-feldspar modeling and thermometry. *American Mineralogist*, *73*, 201–215.

Gerya, T. (2010). *Introduction to numerical geodynamic modelling*. Cambridge University Pres, 345 p. ISBN 978-0-521-88754-0

Hammer, P., Berthet, T., Hetényi, G., Cattin, R., Drukpa, D., Chophel, J., Lechmann, S., Moigne, N. L., Champollion, C., & Doerflinger, E. (2013). Flexure of the India plate underneath the Bhutan Himalaya. *Geophysical Research Letters*, *40*, 4225–4230. https://doi.org/10.1002/grl.50793

Henry, P., Le Pichon, X., & Goffé, B. (1997). Kinematic, thermal and petrological model of the Himalayas: Constraints related to metamorphism within the underthrust Indian crust and topographic elevation. *Tectonophysics*, *273*, 31–56. https://doi.org/10.1016/S0040-1951(96)00287-9

Herman, F., Copeland, P., Avouac, J.-P., Bollinger, L., Mahéo, G., Le Fort, P., Rai, S., Foster, D., Pêcher, A., Stüwe, K., & Henry, P. (2010). Exhumation, crustal deformation, and thermal structure of the Nepal Himalaya derived from the inversion of thermochronological and

thermobarometric data and modeling of the topography. *Journal of Geophysical Research*, *115*, B06407. https://doi.org/10.1029/2008JB006126

Hetényi, G. (2014). To conserve or not to conserve (mass in numerical models). *Terra Nova*, *26*, 372–376. https://doi.org/10.1111/ter.12109

Hetényi, G., Cattin, R., Berthet, T., Le Moigne, N., Chophel, J., Lechmann, S., Hammer, P., Drukpa, D., Sapkota, S. N., Gautier, S., & Thinley, K. (2016). Segmentation of the Himalayas as revealed by arc-parallel gravity anomalies. *Scientific Reports*, *6*, 33866. https://doi.org/10.1038/srep33866

Hetényi, G., Cattin, R., Brunet, F., Vergne, J., Bollinger, L., Nábělek, J. L., & Diament, M. (2007). Density distribution of the India plate beneath the Tibetan Plateau: Geophysical and petrological constraints on the kinetics of lower-crustal eclogitization. *Earth and Planetary Science Letters*, *264*, 226–244. https://doi.org/10.1016/j.epsl.2007.09.036

Hetényi, G., Godard, V., Cattin, R., & Connolly, J. A. D. (2011). Incorporating metamorphism in geodynamic models: The mass conservation problem. *Geophysical Journal International*, *186*, 6–10. https://doi.org/10.1111/j.1365-246X.2011.05052.x

Holland, T., Baker, J., & Powell, R. (1998). Mixing properties and activity-composition relationships of chlorites in the system MgO-FeO-Al_2O_3-SiO_2-H_2O. *European Journal of Mineralogy*, *10*, 395–406. https://doi.org/10.1127/ejm/10/3/0395

Holland, T., & Powell, R. (1996). Thermodynamics of order-disorder in minerals. 2. Symmetric formalism applied to solid solutions. *American Mineralogist*, *81*, 1425–1437.

Holland, T. J. B., & Powell, R. (1998). An internally consistent thermodynamic data set for phases of petrological interest. *Journal of Metamorphic Geology*, *16*, 309–343. https://doi.org/10.1111/j.1525-1314.1998.00140.x

John, T., & Schenk, V. (2003). Partial eclogitisation of gabbroic rocks in a late Precambrian subduction zone (Zambia): Prograde metamorphism triggered by fluid infiltration. *Contributions to Mineralogy and Petrology*, *146*, 174–191. https://doi.org/10.1007/s00410-003-0492-8

Kelly, E. D., Carlson, W. D., & Ketcham, R. A. (2013). Crystallization kinetics during regional metamorphism of porphyroblastic rocks. *Journal of Metamorphic Geology*, *31*, 963–979. https://doi.org/10.1111/jmg.12052

Lavé, J., & Avouac, J.-P. (2000). Active folding of fluvial terraces across the Siwaliks Hills, Himalayas of central Nepal. *Journal of Geophysical Research*, *105*, 5735–5770. https://doi.org/10.1029/1999JB900292

Malvoisin, B., Austrheim, H., Hetényi, G., Reynes, J., Hermann, J., Baumgartner, L. P., & Podladchikov, Y. Y. (2020). Sustainable densification of the deep crust. *Geology*, *48*, 673–677. https://doi.org/10.1130/G47201.1

Malvoisin, B., Podladchikov, Y. Y., & Vrijmoed, J. (2015). Coupling changes in densities and porosity to fluid pressure variations in reactive porous fluid flow: Local thermodynamic equilibrium. *Geochemistry Geophysics Geosystems*, *16*, 4362–4387. https://doi.org/10.1002/2015GC006019

Monsalve, G., Sheehan, A., Schulte-Pelkum, V., Rajaure, S., Pandey, M. R., & Wu, F. (2006). Seismicity and one-dimensional velocity-structure of the Himalayan collision zone: Earthquakes in the crust an upper mantle. *Journal of Geophysical Research*, *111*, B10301. https://doi.org/10.1029/2005JB004062

Nabelek, J., Hetenyi, G., Vergne, J., Sapkota, S., Kafle, B., Jiang, M., Su, H., Chen, J., Huang, B-S.; the Hi-CLIMB Team (2009). Underplating in the Himalaya-Tibet collision zone revealed by the Hi-CLIMB experiment. *Science*, *325*, 1371–1374. https://doi.org/10.1126/science.1167719

Powell, R., & Holland, T. (1999). Relating formulations of the thermodynamics of mineral solid solutions: Activity modeling of pyroxenes, amphiboles, and micas. *American Mineralogist*, *84*, 1–14. https://doi.org/10.2138/am-1999-1-201

Priestley, K., Jackson, J., & McKenzie, D. (2008). Lithospheric structure and deep earthquakes beneath India, the Himalaya and southern Tibet. *Geophysical Journal International*, *172*, 345–362. https://doi.org/10.1111/j.1365-246X.2007.03636.x

Rockow, K. M., Haskin, L. A., Jolliff, B. L., & Fountain, D. (1997). Constraints on element mobility associated with the conversion of granulite to eclogite along fractures in an anorthositic complex on Holsnøy, Norway. *Journal of Metamorphic Geology*, *15*, 401–418.

Roselle, G. T., Baumgartner, L. P., & Chapman, J. A. (1997). Nucleation-dominated crystallization of forsterite in the Ubehebe peak contact aureole, California. *Geology*, *25*, 823–826. https://doi.org/10.1130/0091-7613(1997)025<0823:NDCOFI>2.3.CO;2

Rudnick, R. L., & Fountain, D. M. (1995). Nature and composition of the continental crust—A lower crustal perspective. *Reviews of Geophysics*, *33*, 267–309. https://doi.org/10.1029/95RG01302

Rudnick, R. L., & Gao, S. (2003). Composition of the continental crust. *Treatise on Geochemistry*, *3*, 659.

Schmalholz, S. M., Duretz, T., Hetényi, G., & Medvedev, S. (2019). Distribution and magnitude of stress due to lateral variation of gravitational potential energy between Indian lowland and Tibetan plateau. *Geophysical Journal International*, *216*, 1313–1333. https://doi.org/10.1093/gji/ggy463

Shi, F., Wang, Y., Yu, T., Zhu, L., Zhang, J., Wen, J., Gasc, J., Incel, S., Schubnel, A., Li, Z., Chen, T., Liu, W., Prakapenka, V., & Jin, Z. (2018). Lower-crustal earthquakes in southern Tibet are linked to eclogitization of dry metastable granulite. *Nature Communications*, *9*, 3483. https://doi.org/10.1038/s41467-018-05964-1

Skelton, A. D. L., Bickel, M. J., & Graham, C. M. (1997). Fluid-flux and reaction rate from advective-diffusive carbonation of mafic sill margins in the Dalradian, southwest Scottish Highlands. *Earth and Planetary Science Letters*, *146*, 527–539. https://doi.org/10.1016/S0012-821X(96)00248-8

Subedi, S., Hetényi, G., Vergne, J., Bollinger, L., Lyon-Caen, H., Farra, V., Adhikari, L. B., & Gupta, R. M. (2018). Imaging the Moho and the Main Himalayan Thrust in Western Nepal with receiver functions. *Geophysical Research Letters*, *45*, 13222–13230. https://doi.org/10.1029/2018GL080911

Taetz, S., John, T., Bröcker, M., Spandler, C., & Stracke, A. (2018). Fast intraslab fluid-flow events linked to pulses of high pore fluid pressure at the subducted plate interface. *Earth and Planetary Science Letters*, *482*, 33–43. https://doi.org/10.1016/j.epsl.2017.10.044

Talwani, M., Worzel, J. I., & Landisman, M. (1959). Rapid gravity computations for two-dimensional bodies with application to the Mendocino submarine fracture zone. *Journal of Geophysical Research*, *64*, 46–59. https://doi.org/10.1029/JZ064i001p00049

Toussaint, G., Burov, E., & Jolivet, L. (2004). Continental plate collision: Unstable vs. stable slab dynamics. *Geology*, *32*, 33–36.

Wei, C. J., & Powell, R. (2003). Phase relations in high-pressure metapelites in the system KFMASH (K_2O-FeO-MgO-Al_2O_3-SiO2-H_2O) with application to natural rocks. *Contributions to Mineralogy*

and Petrology, *145*, 301–315. https://doi.org/10.1007/s00410-003-0454-1

White, R. W., Powell, R., Holland, T. J. B., & Worley, B. A. (2000). The effect of TiO_2 and Fe_2O_3 on metapelitic assemblages at greenschist and amphibolite facies conditions: Mineral equilibria calculations in the system K_2O-FeO-MgO-Al_2O_3-SiO_2-H_2O-TiO_2-Fe_2O_3. *Journal of Metamorphic Geology*, *18*, 497–511.

White, R. W., Powell, R., & Phillips, G. N. (2003). A mineral equilibria study of the hydrothermal alteration in mafic greenschist faciesrocks at Kalgoorlie, Western Australia. *Journal of Metamorphic Geology*, *21*, 455–468. https://doi.org/10.1046/j.1525-1314.2003.00454.x

Whittington, A. G., Hofmeister, A. M., & Nabelek, P. I. (2009). Temperature-dependent thermal diffusivity of the Earth's crust and implications for magmatism. *Nature*, *458*, 319–321. https://doi.org/10.1038/nature07818

Wolfe, O. M., & Spear, F. S. (2017). Determining the amount of overstepping required to nucleate garnet during Barrovian regional metamorphism, Connecticut Valley Synclinorium. *Journal of Metamorphic Geology*, *36*, 79–94. https://doi.org/10.1111/jmg.12284

Won, I. J., & Bevis, M. (1987). Computing the gravitational and magnetic anomalies due to a polygon: Algorithms and Fortran subroutines. *Geophysics*, *52*, 232–238. https://doi.org/10.1190/1.1442298

Yamato, P., Agard, P., Burov, E., Le Pourhiet, L., Jolivet, L., & Tiberi, C. (2007). Burial and exhumation in a subduction wedge: Mutual constraints from thermomechanical modeling and natural P-T-t data (Schistes Lustrés, western Alps). *Journal of Geophysical Research*, *112*, B07410. https://doi.org/10.1029/2006JB004441

Zack, T., & John, T. (2007). An evaluation of reactive fluid flow and trace element mobility in subducting slabs. *Chemical Geology*, *239*, 199–216. https://doi.org/10.1016/j.chemgeo.2006.10.020

How to cite this article: Heténi G, Chanard K, Baumgartner LP, Herman F. Metamorphic transformation rate over large spatial and temporal scales constrained by geophysical data and coupled modelling. *J Metamorph Geol*. 2021;39:1131–1143. https://doi.org/10.1111/jmg.12604